





Article

Promising Isotope Effect in Pd₇₇Ag₂₃ for Hydrogen Separation

Francesco Trequattrini ^{1,2}, Oriele Palumbo ², Silvano Tosti ³, Alessia Santucci ³ and Annalisa Paolone ^{2,*}

¹ Dipartimento di Fisica, Sapienza Università di Roma, Piazzale A. Moro 5, I-00185 Rome, Italy; francesco.trequattrini@roma1.infn.it

² Istituto dei Sistemi Complessi, Consiglio Nazionale delle Ricerche, Piazzale A. Moro 5, I-00185 Rome, Italy; oriele.palumbo@roma1.infn.it

³ Dipartimento Fusione e Tecnologie per la Sicurezza Nucleare, ENEA, Via E. Fermi 45, I-00044 Frascati, Italy; silvano.tosti@enea.it (S.T.); alessia.santucci@enea.it (A.S.)

* Correspondence: annalisa.paolone@roma1.infn.it

Abstract: Pd–Ag alloys are largely used as hydrogen separation membranes and, as a consequence, the Pd–Ag–H system has been intensively studied. On the contrary, fewer information is available for the Pd–Ag–D system; thus, the aim of this work is to improve the knowledge of the isotope effect on the commercial Pd₇₇Ag₂₃ alloy, especially for temperature above 200 °C. In particular, deuterium absorption measurements are carried out in the Pd₇₇Ag₂₃ alloy in the temperature range between 79 and 400 °C and in the pressure range between 10^{−2} and 16 bar. In this exploited pressure (p) and composition (c) range, above 300 °C the pc isotherms display the typical shape of materials where only a solid solution of deuterium is present while at lower temperatures these curves seem to be better described by the coexistence of a solid solution and a deuteride in a large composition range. The obtained results are compared and discussed with the ones previously measured with the lightest hydrogen isotope. Such a comparison shows that the Pd₇₇Ag₂₃ alloy exhibits a clear inverse isotope effect, as the equilibrium pressure of the Pd–Ag–D system is higher than in Pd–Ag–H by a factor of ≈2 and the solubility of deuterium is about one half of that of hydrogen. In addition, the absorption measurements were used to assess the deuteration enthalpy that below 300 °C is $\Delta H_{\text{deut}} = 31.9 \pm 0.3$ kJ/mol, while for temperatures higher than 300 °C, ΔH_{deut} increases to 43 ± 1 kJ/mol. Additionally, in this case a comparison with the lighter isotope is given and both deuteration enthalpy values result lower than those reported for hydrogenation. The results described in this paper are of practical interest for applications operating above 200 °C, such as membranes or packing column, in which Pd₇₇Ag₂₃ has to interact with a gas stream containing both hydrogen isotopes.

Keywords: Pd–Ag alloys; metal–hydrogen interactions; thermodynamic assessment; enthalpy of reaction; hydrogen isotope effect



Citation: Trequattrini, F.; Palumbo, O.; Tosti, S.; Santucci, A.; Paolone, A. Promising Isotope Effect in Pd₇₇Ag₂₃ for Hydrogen Separation. *ChemEngineering* **2021**, *5*, 51. <https://doi.org/10.3390/chemengineering5030051>

Academic Editors: Farooq Sher, Andrew S. Paluch and Alirio E. Rodrigues

Received: 28 June 2021

Accepted: 25 August 2021

Published: 27 August 2021

Publisher's Note: MDPI stays neutral with regard to jurisdictional claims in published maps and institutional affiliations.



Copyright: © 2021 by the authors. Licensee MDPI, Basel, Switzerland. This article is an open access article distributed under the terms and conditions of the Creative Commons Attribution (CC BY) license (<https://creativecommons.org/licenses/by/4.0/>).

1. Introduction

It is generally accepted that hydrogen will play an important role in providing future clean and affordable energy in the next years [1]. Although hydrogen produces zero-carbon emissions at the end-use point, it is not a primary source of energy, but it can be easily used as an energy carrier [2,3]. It can be produced starting from different sources, ranging from hydrocarbons to water, or thanks to the metabolism of microbial organisms [4]. It is noteworthy that all the energy chain is effectively “clean and sustainable” only when the hydrogen is produced by renewable energy sources [5,6]. Furthermore, hydrogen is expected to play an important role in the exploitation of the renewable energy sources: due to their intrinsic variability, these energy sources need efficient systems capable of storing energy during the off-peak hours. In a case study focused on Denmark, it was estimated that the excess of electricity could rise to 40% for a wind power penetration of 100% [7]. Hydrogen can be produced from renewable energy via water electrolysis [8] and, after storing, it can be re-used to feed fuel cells [9,10], which produce electricity and water as the only by-product.

Independently of the particular synthesis route, hydrogen is inevitably accompanied by other gases which can be present also in large concentrations [4,11]. Presently, most of the hydrogen is produced via steam reforming of methane and it is foreseeable that still in the mid-term this process will provide the largest share of its production [12]. For these reasons, hydrogen is characterized by the need of separation from impurities (mainly CO₂ and CO). In particular, fuel cells need extremely pure hydrogen, otherwise they become poisoned and their efficiency drastically decreases [4,13]. For this reason, it is necessary to purify the hydrogen gas streams before their exploitation (such as fuel cells and other end-user energy systems). Different technologies are available [13,14], ranging from Pressure Swing Absorption, generally used in large scale industrial plants, to membrane reactors with different active materials, such as metals (crystalline [14] or amorphous [15]), supported metals, porous materials or polymers, that are more suitable and economically convenient for smaller scale applications.

Many metals and metal alloys have been considered for hydrogen purification [16,17]; group V metals (such as Nb, Ta, V) and other metals such as Ni and Pd show a high hydrogen permeability, but they are also prone to hydrogen embrittlement. However, better mechanical properties can be achieved by alloying with other metals, such as Al [16], Fe, Cu [18], Au [19], Ru [20], etc., without affecting too much the overall permeability of the membranes. Among these materials, membranes based on Pd are the most mature technology [21,22].

Pd–Ag self-supported membranes have a long tradition for the purification of hydrogen on a small scale. Various types of permeators and membrane reactors have been proposed for this aim [23,24]. A membrane reactor is a combination of a selective membrane with a catalytic bed and can achieve reaction conversions higher than those of traditional reactors thanks to the well-known “shift effect”. According to Chatelier’s principle, the system in answer to the continuous removal of one of the reaction products (hydrogen in the case of using Pd membranes) makes more feed matter reacting, thus promoting the reaction and realizing high reaction yields [25,26]. Transport mechanisms of both Pd membrane and membrane reactors are based on the same principle: the pressure of a gas containing hydrogen is applied on one side of the membrane; H₂ molecules are split on the exposed metal surface; the hydrogen atoms diffuse in the bulk of the membrane towards the region with a lower hydrogen concentration; finally, they recombine on the surface where a lower pressure of hydrogen is applied. This process is highly selective, as it can occur only for hydrogen (or its isotopes) and not for other molecules. Therefore, gas molecules different from H₂ stay in the mainstream gas, while only hydrogen is selectively transmitted through the membrane towards the permeate stream.

Reactors based on Pd–Ag alloys have had large applications and many technologies have been applied to improve their performances. For example, a different range of pressure of the H₂–N₂ atmosphere has been considered for their application [27] and low temperature bonding has been proved to give good sealing properties [28]. Moreover, on-site repair was exploited [29], various types of nanostructuring of the surfaces were considered [30,31], and the extraction of H₂ from biomaterials was achieved [32].

Pd–Ag alloys with a composition close to Pd₇₇Ag₂₃ display one of the best compromises between the resistance to hydrogen embrittlement and high values of hydrogen permeability [23,32]. Compositions close to the presently investigated ones are practically used for the construction of reactors and permeators [33]. At a microscopic level, the permeability coefficient, Pe , is related to the diffusion coefficient, D , and the solubility, S , of hydrogen in the metal [32]:

$$Pe = D \times S \quad (1)$$

Therefore, it is evident from Equation (1) that metals for hydrogen separation have to exhibit a good compromise between hydrogen solubility and diffusivity. While diffusion coefficients and permeability have been largely investigated for Pd–Ag alloys, especially in the case of hydrogen, much less is known about deuterium and its solubility. Data on isotopic effects are of great importance in order to design the membrane separation units

of the nuclear fusion fuel cycle where hydrogen and its isotopes have to be treated in both gaseous and liquid streams [34]. In addition, the diversity among the H and D behavior in Pd-based materials has also been exploited for the separation of the different hydrogen isotopes. Two major examples are the technique named displacement gas chromatography [35] and the thermal cycles adsorption process (TCAP) [36].

A limited number of previous studies of the isotope effect in Pd–Ag alloys is available in a restricted temperature range for Pd₉₃Ag₇ [37] ($100\text{ °C} < T < 200\text{ °C}$) and for Pd₇₇Ag₂₃ [38] ($101\text{ °C} < T < 146\text{ °C}$). These results evidenced that the absorption properties of deuterium are different from those of hydrogen, concerning the equilibrium pressure between the gas and the solid and the solubility of the hydrogen isotopes. Moreover, in this temperature range, the pressure–composition isotherms are typical of a sample forming a deuteride. However, above 200 °C, no study about the deuterium absorption has been reported and no direct evidence of the occurrence of a solid solution of deuterium or of deuteride in Pd–Ag alloys was proposed.

Additionally, some recent neutron diffraction and spectroscopic studies were limited to a maximum temperature of 200 °C. Neutron diffraction pointed out that deuterium occupies octahedral interstitial sites in the Pd–Ag alloy [39,40]. Moreover, neutron spectroscopy studies investigated the Pd₇₇Ag₂₃ alloys and evidenced that the macroscopic diffusion process is determined by microscopic jump diffusion [41]. It must be noted that all neutron diffraction and/or spectroscopic studies must be conducted in the presence of the heavy deuterium isotope due to its higher cross section. Therefore, it is useful to investigate the solubility properties of deuterium in Pd–Ag alloys and the phase diagram of the Pd–Ag–D system. This information can be obtained by means of pressure–composition isotherms, such as those here reported, and motivated our present investigation.

Moreover, the occurrence of an isotope effect between hydrogen and deuterium, as suggested by the studies of Hara et al. [37] and Anand et al. [38], is the prerequisite to obtain a different concentration of the hydrogen isotopes in the gas emitted by the reactor for hydrogen purification, due to the possible different values of diffusion coefficient and solubility of the isotope in the metal (see Equation (1)). Additionally, in this respect, it is interesting to evidence the possible differences between the two hydrogen isotopes regarding their solubility in the Pd₇₇Ag₂₃ alloy.

In order to deepen the knowledge of the absorption of deuterium in the Pd₇₇Ag₂₃ alloy, in particular to provide initial information about the phase diagram of the Pd₇₇Ag₂₃–D system, as well as to measure the equilibrium pressure between the alloy and deuterium and the deuteration enthalpy, we performed measurements of the pressure–composition isotherms as a function of temperature, between 79 and 400 °C, and as a function of pressure, between 10^{-2} and 16 bar. Moreover, we directly compared the obtained pressure–composition isotherms with those measured on the same sample in the presence of the light hydrogen isotope.

2. Materials and Methods

The sample used for this study was a commercial Pd₇₇Ag₂₃ (wt%) foil with a thickness of 25 µm, purchased from Goodfellow. We intentionally used a commercial alloy in order to obtain results closer to applications; indeed, such material was used for the construction of real permeators [32,33]. A surface analysis of the sample was performed by the SEM/EDX technique, as reported in Ref. [42], and it confirmed the correct stoichiometry and the absence of impurities, besides some organic compounds on the surface. A piece with dimensions ~20 mm × 5 mm and mass ~148 mg was cut from the foil, gently cleaned with ethanol and used for deuterium sorption measurements in a homemade Sieverts apparatus [43,44] in the temperature range 79–400 °C. The alloy was heated up at 400 °C in vacuum and exposed to a high pressure (15 bar) of hydrogen/deuterium in order to activate the surface for the sorption experiments. A few hydrogenation/dehydrogenation cycles were performed in order to be sure of good sorption properties and fast kinetics. Finally, the absorbed gas was removed by pumping overnight by means of a turbo pump

($p < 10^{-4}$ mbar in the sample holder) and by checking that no release of gas was observed from the sample after this treatment. The same type of discharge procedure was used after the construction of each absorption isotherm. For the present study the inlet of deuterium gas was upgraded and it was possible to apply a maximum D_2 pressure of ≈ 17 bar, to be compared to the previous reported maximum of ≈ 2 bar [42]. Deuterium gas (purity > 99%) was purchased from Società Italiana Acetilene e Derivati (Rome, Italy). The sample here investigated was the same previously used in Ref. [42] for the measures of hydrogen sorption. The reproducibility of the measurements was evaluated by repeating measurements at selected points of the isotherms. Moreover, two isotherms were measured twice. The overall uncertainties on the experimental points are smaller than the symbols used in the figures.

3. Results and Discussion

In the following, we report the results of our experimental investigation divided into three subsections focusing on the deuterium absorption pressure–composition isotherms (Section 3.1), the evidence of a hydrogen isotope effect (Section 3.2) and, finally, a thermodynamic assessment of the deuteration enthalpy (Section 3.3) discussed also in comparison with results on similar alloys.

3.1. Deuterium Absorption in $Pd_{77}Ag_{23}$

The absorption of deuterium in $Pd_{77}Ag_{23}$ was measured between 79 and 400 °C in the pressure range between 10^{-2} and 16 bar. Figure 1 reports the pressure–composition isotherms at selected temperatures in a double logarithmic scale, compared to those previously measured for the same sample with hydrogen gas [42]. The deuterium/hydrogen concentration is expressed as D/M or H/M, i.e., number of deuterium or hydrogen atoms per metal atom [45].

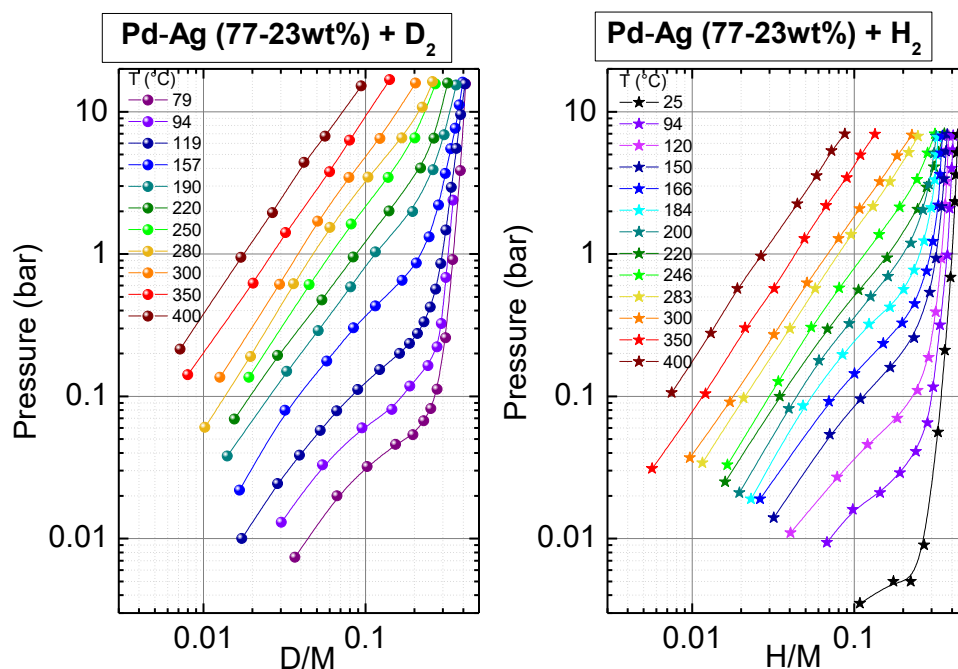


Figure 1. Absorption pressure–composition isotherms measured at selected temperatures for $Pd_{77}Ag_{23}$ with D_2 (left) and H_2 (right) gas.

As expected, the solubility of deuterium in the sample at a fixed pressure increased as the temperature decreased; for example, for $p = 1$ bar D/M was ≈ 0.02 at 400 °C and ≈ 0.35 at 79 °C. Moreover, one can easily appreciate a clear qualitative difference between the curves measured for $T < 300$ °C and $T \geq 300$ °C in the investigated pressure range.

In the higher temperature regime, one observes straight lines, that is a linear dependence between $\ln(p)$ and $\ln(D/M)$. This fact assured the validity of the Sieverts law ($p \sim (D/M)^n$) in the present case for $T \geq 300$ °C [46]. The Sieverts law is expected to hold when deuterium (or hydrogen) are diluted in materials, i.e., they are dissolved in a solid in the form of a solid solution (usually called α phase), without the formation of a deuteride (or hydride) (also called β phase) [47]. Conversely, for temperature values lower than 300 °C, the isotherm curves were convex and displayed a large increase in the pressure for $D/M \geq 0.2$. These facts can be related to the occurrence of the formation of a deuteride. It must be noted that the presently reported measurements extended only up to a pressure of 16 bar; the occurrence of a curve behavior compatible with a deuteride phase above 300 °C and at a pressure higher than 16 bar was, therefore, not excluded.

The values of the equilibrium pressure obtained in the present case were well compatible with those reported in Ref. [38] for a Pd₇₇Ag₂₃ foil produced by arc melting. Those authors reported that the equilibrium pressure, P_{eq} , for deuterium at 389 K (116 °C) for $D/M = 0.20$ was about 0.20 bar. In the presently investigated sample, for $T = 119$ °C and $D/M = 0.20P_{eq}$ was 0.23 bar.

To the best of our knowledge a detailed phase diagram of the Pd₇₇Ag₂₃-H (D) system is not yet reported; however, some indications are available from the literature. Pure palladium forms hydrides or deuterides below 290 and 283 °C, respectively [48,49], while above these temperatures only a solid solution can be observed. Some pressure–composition curves for Pd₉₃Ag₇ [37] between 100 and 200 °C and for Pd₇₇Ag₂₃ [38] between 101 and 146 °C displayed the typical shape for the formation of a deuteride. Further studies at higher temperatures are not available. Neutron diffraction studies of Pd_{77.2}Ag_{22.8}D_v evidenced also that two FCC crystal structures coexist in a large temperature–pressure range suggesting the transition from a solid solution (α phase) to a deuteride (β phase) below 200 °C, the maximum temperature of that study [40].

3.2. Hydrogen Isotope Effect in Pd₇₇Ag₂₃

For the presently studied composition, the comparison of the pressure–composition isotherms measured for deuterium absorption with those previously reported for hydrogen [42], shown in Figure 1, indicated the occurrence of a clear isotope effect that was visible in the whole temperature range. Indeed, the equilibrium pressure for deuterium was higher than for hydrogen at the same temperature and composition; equivalently, a lower deuterium solubility was observed at a selected temperature and pressure compared to the solubility of hydrogen. For example, at $T = 300$ °C and $p = 1$ bar, the solubility of deuterium was $D/M = 0.04$, while that of hydrogen was $H/M = 0.07$; alternatively, at $T = 300$ °C and $H/M = 0.04$, one had an equilibrium pressure of ≈ 0.37 bar instead of 1 bar for D₂. Moreover, at $T = 220$ °C and $p = 1$ bar, the solubility of deuterium was $D/M = 0.09$ while that of hydrogen was $H/M = 0.16$; alternatively, at $T = 220$ °C and $H/M = 0.09$, one had an equilibrium pressure of ≈ 0.42 bar instead of 1 bar for D₂.

We want to point out that, to the best of our knowledge, no previous investigation of the absorption of deuterium in Pd–Ag alloys is available above 200 °C. Indeed, the previous reports about the hydrogen isotope effect in Pd–Ag alloys concerned Pd₉₃Ag₇ [37] (100 °C $< T < 200$ °C) and Pd₇₇Ag₂₃ [38] (101 °C $< T < 146$ °C), both samples investigated in the deuteride form. Anand reported a factor of three between the equilibrium pressure for deuterium compared to hydrogen for a composition of about 0.2 [37]. For a similar composition, in the case of the dehydrogenation of Pd₇₇Ag₂₃, a factor between two and three was reported for the ratio between the equilibrium pressure of deuterium and hydrogen [38]. This value compared well with that obtained for the presently investigated sample.

This type of isotope effect is usually called “inverse” because the equilibrium pressure for deuterium is higher than in the case of hydrogen or, equivalently, the solubility of deuterium is lower than for hydrogen. This fact was already reported for Pd [48,49] and for Pd₉₃Ag₇ [37], Pd₇₇Ag₂₃ [38] and Pd₇₅Ag₂₅ [50] measured in a more restricted temperature range. At a microscopic level, the occurrence of normal or inverse isotope

effects in different materials depends on the different types of interstitial sites occupied by hydrogen/deuterium [51,52] in the specific metal/alloy. In general, a wide number of investigations of pure metals conducted to rationalize that materials where hydrogen and its isotopes occupy tetrahedral interstitial sites displayed a normal isotope effect, while samples where hydrogen was stored in octahedral sites showed an inverse isotope effect [51]. In fact, octahedral interstitial sites correspond to broad flat energy potentials; on the contrary, tetrahedral sites have steep and narrow energy profiles [51,52]. As a consequence, the zero-point vibrational energy of tetrahedral sites (≈ 150 meV) is much higher than that of octahedral ones (≈ 50 meV). Therefore, the energy difference between the energy levels of gaseous hydrogen and a solid with octahedral interstitial sites is lower than in the case of deuterium and the solubility of hydrogen in this case is higher than that of deuterium (“inverse isotope effect”) [51,52]. The opposite holds in the case of tetrahedral interstitial sites being available (“normal isotope effect”) [51,52]. Regarding pure metals, the benchmarks of a normal and inverse isotope effect are vanadium and palladium, respectively [51]. Usually the occurrence of the same type of isotope effect is retained also in alloys of these metals [53,54]. The occurrence of the inverse isotope effect in Pd₇₇Ag₂₃ here reported was perfectly in line with the occupancy of octahedral interstitial sites recently evidenced by means of neutron diffraction measurements [39,40].

3.3. Enthalpy of Deuteration

From the absorption isotherms reported in Figure 1, it is possible to evaluate the enthalpy of deuteration of the Pd₇₇Ag₂₃ alloy, ΔH_{deut} . Figure 2 reports the Van't Hoff plot of the logarithm of the equilibrium pressure between the gas and the solid as a function of the inverse of the temperature. Many crystalline samples displayed almost an horizontal plateau of the equilibrium pressure vs. composition. This was the case, for example, of MgH₂ [55] and its alloys [56], and for annealed alloys derived from LaNi₅ [57]. The isotherms reported in Figure 1 did not display any horizontal plateau. However, also in the case of non-flat pressure–composition isotherms, one can still use the Van't Hoff plot to calculate the deuteration enthalpy, provided that one uses the pressure values measured for a fixed D/M content [58,59]. In the present case, the analysis was performed at three different D/M values (0.02, 0.04 and 0.10) in order to check whether changes of ΔH_{deut} as a function of D/M could be observed. Two different slopes could be identified below and above ≈ 300 °C ($1000/T(K) \approx 1.771/K$). At lower temperatures, one obtains $\Delta H_{\text{deut}} = 31.9 \pm 0.3$ kJ/mol, while for temperatures higher than 300 °C $\Delta H_{\text{deut}} = 43 \pm 1$ kJ/mol. These values were obtained as the mean of the figures calculated at three D/M concentrations which did not differ for more than 2 kJ/mol in the same temperature regime. The fact that one clearly observes two different deuteration enthalpy values further corroborates the idea that two different thermodynamic states are observable at low and high temperatures. Here, they were interpreted as a deuterium solid solution at high T and the coexistence of a solid solution and a deuteride at lower temperatures, at least in the investigated pressure range. It can be noticed that the deuteration enthalpy was higher for high temperatures where only an α phase was observed. This fact was already reported for the same alloy subject to the absorption of hydrogen [42] and for the absorption of hydrogen in pure Pd ($\Delta H_{\text{hydr}}(\alpha \text{ phase}) = 20.6 \pm 0.3$ kJ/(1/2 mol H₂), $\Delta H_{\text{hydr}}(\alpha \text{ to } \beta \text{ phase}) = 18.7 \pm 0.2$ kJ/(1/2 mol H₂)) [48]. It was previously evidenced that in pure Pd, a key role for the absorption of interstitial hydrogen is played by the formation of dislocations [48]. Hydrogen interacts with the dislocations and the chemical potential of the H interstitials is modified by the elastic interactions with the stress field of the dislocations [48]. Both values of ΔH obtained in the case of deuteration are lower than those obtained for hydrogenation; in fact, for hydrogenation $\Delta H_{\text{hydr}} = 49 \pm 2$ kJ/mol for low concentration and high temperature and 43 ± 2 kJ/mol for low temperatures and higher concentrations. A direct comparison of the Van't Hoff plot of the Pd₇₇Ag₂₃–D and Pd₇₇Ag₂₃–H systems is reported in Figure S1 of the Supplementary Material. The lower enthalpy for deuteration than for hydrogenation was previously reported by Hara et al. for Pd₉₃Ag₇ [37] (the enthalpy

changed for the desorption of hydrogen and deuterium were evaluated to be 43.0 kJ/mol and 36.4 kJ/mol, respectively), Lässer for Pd₉₀Ag₁₀ [60], and it is well known for pure Pd ($\Delta H_{\text{hydr}} = 40.2$ kJ/mol, $\Delta H_{\text{deut}} = 35.1$ kJ/mol) [61,62]. For an easier visualization of the values of hydrogenation/deuteration enthalpy, they are reported in Table 1, with a comparison of the literature data for the above-mentioned literature values. It must be noted that the values reported in Ref. [48] was referred to $\frac{1}{2}$ mol H₂ and not to 1 mol H₂, as reported in the other cases, so that for comparison purposes they were doubled in Table 1.

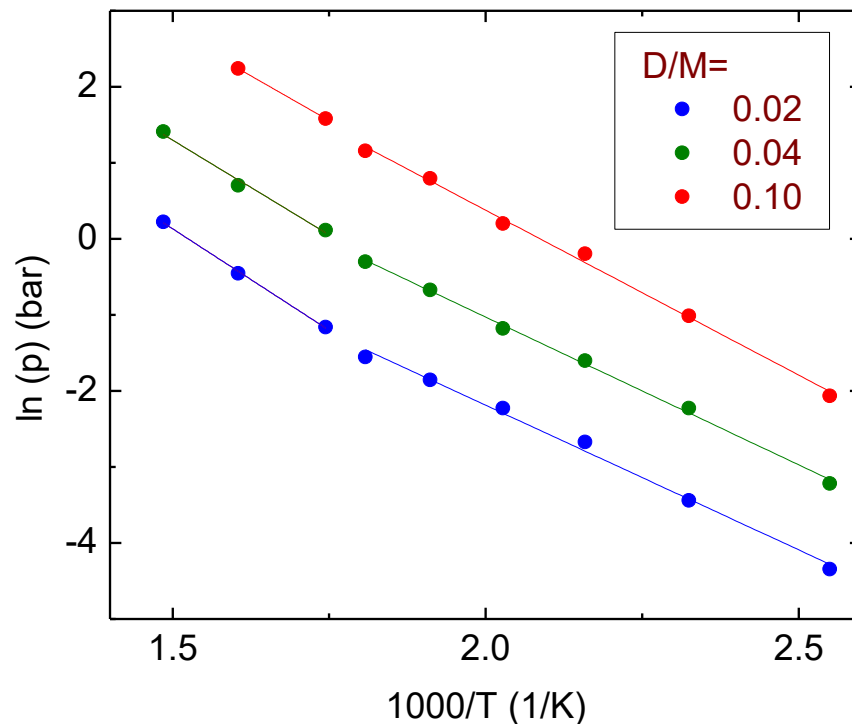


Figure 2. Van't Hoff plot for Pd₇₇Ag₂₃ at fixed D/M (the number of deuterium atoms per atom of metal) and best fit lines to calculate the hydrogenation enthalpy.

Table 1. Comparison of the hydrogenation/deuteration enthalpy values (in kJ/mol) for the presently investigated Pd₇₇Ag₂₃ sample with those of similar Pd-based materials. Uncertainties are reported where available from the literature data.

Material	Hydrogenation α Phase	Hydrogenation β Phase	Deuteration α Phase	Deuteration β Phase
Pd	41.2 \pm 0.6 [48]	37.4 \pm 0.4 [48]		
Pd	40.2 [61]		35.1 [61,62]	
Pd ₉₃ Ag ₇		43.0 [37]		36.4 [37]
Pd ₉₀ Ag ₁₀		42.4 [37]		38.9 [37]
Pd ₇₇ Ag ₂₃	49 \pm 2 [42]	43 \pm 2 [42]	43 \pm 1	31.9 \pm 0.3

4. Conclusions

The solubility of deuterium in the Pd₇₇Ag₂₃ alloy was investigated using a Sieverts experimental setup. The shape of the isothermal pressure–composition curves suggested that below 16 bar and above 300 °C only a solid solution phase exists, while below such a temperature the coexistence of a solid solution with a deuteride is more likely. These different thermodynamic states were further supported by the different deuteration enthalpy measured in the two temperature regimes. The present data did not exclude that a deuteride can form above 300 °C at pressures higher than those here investigated.

Comparing the isotherms with those obtained for the absorption of hydrogen, one clearly observes an inverse isotope effect, witnessed by the higher equilibrium pressure of D₂ with respect to H₂ and the lower solubility of the heavier isotope. The deuteration enthalpy values calculated for the α and β phases were lower than those obtained for hydrogenation. Future work will be devoted to the investigation of the isotope effect in Pd-based alloys with different chemical substitutions.

The presently reported values of the equilibrium pressure of Pd₇₇Ag₂₃ are of great interest for practical systems, such as membranes and packing columns, in which the gas stream to be treated contains both hydrogen isotopes. In fact, the two isotopes will differently dissolve in the alloy and, therefore, they will be differently transferred through the material. We provided a quantitative description of the isotope effect and a microscopic explanation for its occurrence.

Membrane applications in the fusion fuel cycle could benefit from the improved separation efficiency coming from the study of alloying of Pd with a different Ag content or with different elements (Cu, Ti, etc.). In parallel, the development of alloys with a low Pd content will have the scope of reducing the cost of the separation units (both membranes and membrane reactors) to be used in the hydrogen purification processes needed to make actual the future hydrogen economy.

Supplementary Materials: The following are available online at <https://www.mdpi.com/article/10.3390/chemengineering5030051/s1>, Figure S1. Comparison of the Van't Hoff plots for Pd₇₇Ag₂₃-D (present work) and Pd₇₇Ag₂₃-H systems.

Author Contributions: Conceptualization, A.P. and S.T.; methodology, A.P., S.T. and A.S.; validation, F.T., O.P. and A.P.; formal analysis, A.P.; investigation, F.T., O.P. and A.P.; resources, S.T. and A.S.; writing—original draft preparation, A.P.; visualization, A.P. All authors have read and agreed to the published version of the manuscript.

Funding: This research received no external funding.

Institutional Review Board Statement: Not applicable.

Informed Consent Statement: Not applicable.

Data Availability Statement: Data are contained within the article or Supplementary Material.

Conflicts of Interest: The authors declare no conflict of interest.

References

1. IEA. The Future of Hydrogen. Available online: <https://www.iea.org/reports/the-future-of-hydrogen> (accessed on 23 June 2021).
2. Dawood, F.; Anda, M.; Shafiullah, G. Hydrogen production for energy: An overview. *Int. J. Hydrog. Energy* **2020**, *45*, 3847–3869. [[CrossRef](#)]
3. International Energy Agency (IEA). *World Energy Outlook Report OECD/IEA 2014*; International Energy Agency (IEA): Paris, France, 2014; Available online: <https://www.iea.org/reports/world-energy-outlook-2014> (accessed on 29 July 2021).
4. Du, Z.; Liu, C.; Zhai, J.; Guo, X.; Xiong, Y.; Su, W.; He, G.A. Review of Hydrogen Purification Technologies for Fuel Cell Vehicles. *Catalysts* **2021**, *11*, 393. [[CrossRef](#)]
5. Dincer, I.; Acar, C. Innovation in hydrogen production. *Int. J. Hydrog. Energy* **2017**, *42*, 14843–14864. [[CrossRef](#)]
6. Southall, G.D.; Khare, A. The feasibility of distributed hydrogen production from renewable energy sources and the financial contribution from UK motorists on environmental grounds. *Sustain. Cities Soc.* **2016**, *26*, 134–149. [[CrossRef](#)]
7. Jørgensen, C.; Ropenus, S. Production price of hydrogen from grid connected electrolysis in a power market with high wind penetration. *Int. J. Hydrog. Energy* **2008**, *33*, 5335–5344. [[CrossRef](#)]
8. Kirati, S.; Hammoudi, M.; Mousli, I. Hybrid energy system for hydrogen production in the Adrar region (Algeria): Production rate and purity level. *Int. J. Hydrog. Energy* **2018**, *43*, 3378–3393. [[CrossRef](#)]
9. Staffell, I.; Scamman, D.; Velazquez Abad, A.; Balcombe, P.; Dodds, P.E.; Ekins, P.; Shah, N.; Ward, K.R. The role of hydrogen and fuel cells in the global energy system. *Energy Environ. Sci.* **2019**, *12*, 463–491. [[CrossRef](#)]
10. Marchenko, O.; Solomin, S. Modeling of hydrogen and electrical energy storages in wind/PV energy system on the Lake Baikal coast. *Int. J. Hydrog. Energy* **2017**, *42*, 9361–9370. [[CrossRef](#)]
11. Wunsch, A.; Gapp, E.; Peters, T.; Pfeifer, P. Impact of product gas impurities from dehydrogenation of perhydro-dibenzyltoluene on the performance of a 10 μ m Pd Ag-membrane. *J. Membr. Sci.* **2021**, *628*, 119094. [[CrossRef](#)]

12. IEA. World Energy Outlook 2016. Available online: <https://www.iea.org/reports/world-energy-outlook-2016> (accessed on 29 July 2021).
13. Alique, D.; Martinez-Diaz, D.; Sanz, R.; Calles, J.A. Review of supported Pd-based membranes preparation by electroless plating for ultra-pure hydrogen production. *Membranes* **2018**, *8*, 5. [[CrossRef](#)]
14. Ockwig, N.W.; Nenoff, T.M. Membranes for hydrogen separation. *Chem. Rev.* **2007**, *107*, 4078–4110. [[CrossRef](#)]
15. Sarker, S.; Chandra, D.; Hirscher, M.; Dolan, M.; Isheim, D.; Wermer, J.; Viano, D.; Baricco, M.; Udovic, T.J.; Grant, D.; et al. Developments in the Ni–Nb–Zr amorphous alloy membranes. *Appl. Phys. A* **2016**, *122*, 1–9. [[CrossRef](#)]
16. Phair, J.W.; Donelson, R. Developments and design of novel (non-palladium-based) metal membranes for hydrogen separation. *Ind. Eng. Chem. Res.* **2006**, *45*, 5657–5674. [[CrossRef](#)]
17. Santucci, A.; Tosti, S.; Basile, A. Alternatives to palladium in membranes for hydrogen separation: Nickel, niobium and vanadium alloys, ceramic supports for metal alloys and porous glass membranes. In *Handbook of Membrane Reactors*; Basile, A., Ed.; (Ch. 4); Woodhead Publishing Series in Energy: Cornwall, UK, 2013; Volume 1, pp. 183–217. [[CrossRef](#)]
18. Zhao, C.; Sun, B.; Jiang, J.; Xu, W. H₂ purification process with double layer bcc-PdCu alloy membrane at ambient temperature. *Int. J. Hydrog. Energy* **2020**, *45*, 17540–17547. [[CrossRef](#)]
19. De Nooijer, N.; Sanchez, J.D.; Melendez, J.; Fernandez, E.; Tanaka, D.A.P.; Annaland, M.V.S.; Gallucci, F. Influence of H₂S on the hydrogen flux of thin-film PdAgAu membranes. *Int. J. Hydrog. Energy* **2020**, *45*, 7303–7312. [[CrossRef](#)]
20. Liu, J.; Bellini, S.; de Nooijer, N.C.A.; Sun, Y.; PachecoTanaka, D.A.; Tang, C.; Li, H.; Gallucci, F.; Caravella, A. Hydrogen permeation and stability in ultra-thin PdRu supported membranes. *Int. J. Hydrog. Energy* **2020**, *45*, 7455–7467. [[CrossRef](#)]
21. Bellini, S.; Liang, X.; Li, X.; Gallucci, F.; Caravella, A. Non-ideal hydrogen permeation through V-alloy membranes. *J. Membr. Sci.* **2018**, *564*, 456–464. [[CrossRef](#)]
22. Li, H.; Caravella, A.; Xu, H.Y. Recent progress in Pd-based composite membranes. *J. Mater. Chem. A* **2016**, *4*, 14069–14094. [[CrossRef](#)]
23. Basile, A.; Gallucci, F.; Tosti, S. Synthesis, characterization, and applications of palladium membranes. *Membr. Sci. Technol.* **2008**, *13*, 255–323. [[CrossRef](#)]
24. Tanaka, D.A.P.; Medrano, J.A.; Viviente Sole, J.L.; Gallucci, F. Metallic membranes for hydrogen separation. In *Current Trends and Future Developments on (Bio-) Membranes*; Basile, A., Gallucci, F., Eds.; Elsevier: Amsterdam, The Netherlands, 2020; pp. 1–29.
25. Shu, J.; Grandjean, B.P.A.; Van Neste, A.; Kaliaguine, S. Catalytic palladium-based membrane reactors: A review. *Can. J. Chem. Eng.* **1991**, *69*, 1036–1060. [[CrossRef](#)]
26. Kikuchi, E. Membrane reactor application to hydrogen production. *Catal. Today* **2000**, *56*, 97–101. [[CrossRef](#)]
27. Chen, W.-H.; Escalante, J. Influence of vacuum degree on hydrogen permeation through a Pd membrane in different H₂/N₂ gas mixtures. *Renew. Energy* **2020**, *155*, 1245–1263. [[CrossRef](#)]
28. Oh, D.-K.; Lee, K.-Y.; Park, J.-S. Hydrogen Purification from compact palladium membrane module using a low temperature diffusion bonding technology. *Membranes* **2020**, *10*, 338. [[CrossRef](#)] [[PubMed](#)]
29. Ma, Y.; Tang, C.; Bao, F.; Shao, W.; Xu, T.; Li, H.; Xu, H. Microstructural investigation and on-site repair of thin pd-ag alloy membranes. *Membranes* **2020**, *10*, 384. [[CrossRef](#)] [[PubMed](#)]
30. Petriev, I.; Pushankina, P.; Bolotin, S.; Lutsenko, I.; Kukueva, E.; Baryshev, M. The influence of modifying nanoflower and nanostar type Pd coatings on low temperature hydrogen permeability through Pd-containing membranes. *J. Membr. Sci.* **2021**, *620*, 118894. [[CrossRef](#)]
31. Petriev, I.; Pushankina, P.; Lutsenko, I.; Shostak, N.; Baryshev, M. Synthesis, electrocatalytic and gas transport characteristics of pentagonally structured star-shaped nanocrystallites of Pd-Ag. *Nanomaterials* **2020**, *10*, 2081. [[CrossRef](#)]
32. Tosti, S.; Cavezza, C.; Fabbicino, M.; Pontoni, L.; Palma, V.; Ruocco, C. Production of hydrogen in aPd-membrane reactor via catalytic reforming of olive mill wastewater. *Chem. Eng. J.* **2015**, *275*, 366–373. [[CrossRef](#)]
33. Vadrucci, M.; Borgognoni, F.; Moriani, A.; Santucci, A.; Tosti, S. Hydrogen permeation through Pd–Ag membranes: Surface effects and Sieverts’ law. *Int. J. Hydrog. Energy* **2013**, *38*, 4144–4152. [[CrossRef](#)]
34. Tosti, S.; Pozio, A. Membrane processes for the nuclear fusion fuel cycle. *Membranes* **2018**, *8*, 96. [[CrossRef](#)] [[PubMed](#)]
35. Deng, X.; Luo, D.; Qin, X.; Yang, W. Hydrogen isotopes separation using frontal displacement chromatography with Pd–Al₂O₃ packed column. *Int. J. Hydrog. Energy* **2012**, *37*, 10774–10778. [[CrossRef](#)]
36. Heung, L.K.; Sessions, H.T.; Poore, A.S.; Jacobs, W.D.; Williams, C.S. Next generation TCAP hydrogen isotope separation process. *Fusion Sci. Technol.* **2008**, *54*, 399–402. [[CrossRef](#)]
37. Hara, M.; Sakurai, J.; Akamaru, S.; Hashizume, K.; Nishimura, K.; Mori, K.; Okabe, T.; Watanabe, K.; Matsuyama, M. Thermodynamic and magnetic properties of Pd_{0.93}Ag_{0.07} hydride. *Mater. Trans.* **2007**, *48*, 3154–3159. [[CrossRef](#)]
38. Anand, N.; Pati, S.; Jat, R.A.; Parida, S.; Mukerjee, S. Thermodynamics and kinetics of hydrogen/deuterium absorption–desorption in Pd 0.77 Ag 0.23 alloy. *Int. J. Hydrog. Energy* **2015**, *40*, 444–450. [[CrossRef](#)]
39. Catti, M.; Fabelo, O.; Filabozzi, A.; Pietropaolo, A.; Tosti, S.; Pozio, A.; Santucci, A. Neutron diffraction study of the Pd_{0.772}Ag_{0.228}Dv membrane for hydrogen separation. *Int. J. Hydrog. Energy* **2017**, *42*, 6787–6792. [[CrossRef](#)]
40. Catti, M.; Fabelo, O.; Filabozzi, A.; Pietropaolo, A.; Santucci, A.; Tosti, S. Kinetics of deuteration of the Pd_{0.772}Ag_{0.228} alloy with α/β phase transition by in-situ neutron diffraction. *J. Alloys. Compd.* **2019**, *790*, 502–508. [[CrossRef](#)]
41. Colognesi, D.; Demmel, F.; Filabozzi, A.; Pietropaolo, A.; Pozio, A.; Romanelli, G.; Santucci, A.; Tosti, S. Proton dynamics in palladium–silver: An inelastic neutron scattering investigation. *Molecules* **2020**, *25*, 5587. [[CrossRef](#)]

42. Paolone, A.; Tosti, S.; Santucci, A.; Palumbo, O.; Trequattrini, F. Hydrogen and deuterium solubility in commercial Pd–Ag alloys for hydrogen purification. *Chem. Eng.* **2017**, *1*, 14. [[CrossRef](#)]
43. Palumbo, O.; Brutti, S.; Trequattrini, F.; Sarker, S.; Dolan, M.; Chandra, D.; Paolone, A. Temperature dependence of the elastic modulus of (Ni_{0.6}Nb_{0.4})_{1-x}Zr_x membranes: Effects of thermal treatments and hydrogenation. *Energies* **2015**, *8*, 3944–3954. [[CrossRef](#)]
44. Palumbo, O.; Trequattrini, F.; Vitucci, F.M.; Bianchin, A.; Paolone, A. Study of the hydrogenation/dehydrogenation process in the Mg–Ni–C–Al system. *J. Alloys Compd.* **2015**, *645*, S239–S241. [[CrossRef](#)]
45. Palumbo, O.; Trequattrini, F.; Sarker, S.; Hulyakar, M.; Pal, N.; Chandra, D.; Dolan, M.; Paolone, A. New studies of the physical properties of metallic amorphous membranes for hydrogen purification. *Challenges* **2017**, *8*, 4. [[CrossRef](#)]
46. Gupta, C.K. *Chemical Metallurgy: Principles and Practice*; Wiley-VCH: Weinheim, Germany, 2003; p. 273.
47. Suzuki, A.; Yukawa, H. A Review for consistent analysis of hydrogen permeability through dense metallic membranes. *Membranes* **2020**, *10*, 120. [[CrossRef](#)] [[PubMed](#)]
48. Manchester, F.D.; Martin, A.S.; Pitre, J.M. The H–Pd (hydrogen–palladium) system. *J. Phase Equilibria Diffus.* **1994**, *15*, 62–83. [[CrossRef](#)]
49. Wicke, E.; Blaurock, J. New experiments on and interpretations of hysteresis effects of Pd–D₂ and Pd–H₂. *J. Less Common Met.* **1987**, *130*, 351–363. [[CrossRef](#)]
50. Serra, E.; Kemali, M.; Perujo, A.; Ross, D.K. Hydrogen and deuterium in Pd–25 Pct Ag alloy: Permeation, diffusion, solubilization, and surface reaction. *Metall. Mater. Trans. A* **1998**, *29*, 1023–1028. [[CrossRef](#)]
51. Sicking, G. Isotope effects in metal–hydrogen systems. *J. Less Common Met.* **1984**, *101*, 169–190. [[CrossRef](#)]
52. Wiswall, R.H.; Reilly, J.J. Inverse hydrogen isotope effects in some metal hydride systems. *Inorg. Chem.* **1972**, *11*, 1691–1696. [[CrossRef](#)]
53. Bellini, S.; Sun, Y.; Gallucci, F.; Caravella, A. Thermo dynamic aspects in non-ideal metal membranes for hydrogen purification. *Membranes* **2018**, *8*, 82. [[CrossRef](#)]
54. Brutti, S.; Tosti, S.; Santucci, A.; Paolone, A. Deuterium absorption properties of V₈₅Ni₁₅ and evidence of isotope effect. *Int. J. Hydrog. Energy* **2019**, *44*, 20145–20149. [[CrossRef](#)]
55. El-Eskandarany, M.; Shaban, E.; Ali, N.; Aldakheel, F.; Alkandary, A. In-situ catalyzation approach for enhancing the hydrogenation/dehydrogenation kinetics of MgH₂ powders with Ni particles. *Sci. Rep.* **2016**, *6*, 37335. [[CrossRef](#)]
56. Brutti, S.; Farina, L.; Trequattrini, F.; Palumbo, O.; Reale, P.; Silvestri, L.; Panero, S.; Paolone, A. Extremely pure Mg₂FeH₆ as a negative electrode for lithium batteries. *Energies* **2018**, *11*, 1952. [[CrossRef](#)]
57. Pinatel, E.R.; Palumbo, M.; Massimino, F.; Rizzi, P.; Baricco, M. Hydrogen sorption in the LaNi_{5-x}Al_x-H system (0 ≤ x ≤ 1). *Intermetallics* **2015**, *62*, 7–16. [[CrossRef](#)]
58. Karger, B.L.; Snyder, L.R.; Horvath, C. *An Introduction to Separation Science*; Wiley: New York, NY, USA, 1973.
59. Palumbo, O.; Trequattrini, F.; Pal, N.; Hulyakar, M.; Sarker, S.; Chandra, D.; Flanagan, T.; Dolan, M.; Paolone, A. Hydrogen absorption properties of amorphous (Ni_{0.6}Nb_{0.4-y}Ta_y)_{100-x}Zr_x membranes. *Prog. Nat. Sci.* **2017**, *27*, 126–131. [[CrossRef](#)]
60. Lässer, R. Tritium in Metals. *Z. Phys. Chem. Neue Folge* **1985**, *143*, 23–49. [[CrossRef](#)]
61. Yasumatsu, T.; Wan, J.L.; Matsuyama, M.; Watanabe, K. Absorption of hydrogen isotopes by Pd–Pt alloys. *J. Alloys Compd.* **1999**, *293–295*, 900–907. [[CrossRef](#)]
62. Carson, A.W.; Lewis, F.A. Pressure–composition isotherms for the Pd + Ag + H system. *Trans. Faraday Soc.* **1967**, *63*, 1453–1457. [[CrossRef](#)]